Eur. Phys. J. Special Topics **227**, 603–614 (2018)

https://doi.org/10.1140/epjst/e2018-00138-1

THE EUROPEAN PHYSICAL JOURNAL SPECIAL TOPICS

Regular Article

Interactions between a locally separating stable manifold and a bursting periodic orbit

S. Farjami, V. Kirk, and H.M. Osinga[a]

Department of Mathematics, The University of Auckland, Private Bag 92019, Auckland 1142, New Zealand

Received 21 December 2017 / Received in final form 16 April 2018
Published online 4 October 2018

Abstract. Multi-spike bursting of the membrane potential is understood to be a key mechanism for cell signalling in neurons. During the active phase of a burst, the voltage potential across the cell membrane exhibits a series of spikes. This is followed by a silent (recovery) phase during which there is relatively little change in the potential. Mathematical models of this behaviour are frequently based on Hodgkin–Huxley formalism; the dynamics of the voltage is expressed in terms of ionic currents that lead to a system of ordinary differential equations in which some variables (voltage, in particular) are fast and others are slow. The bursting patterns observed in such slow-fast models are often explained in terms of transitions between different coexisting attracting states associated with the so-called fast subsystem, for which the slow variables are viewed as parameters. In particular, the threshold that determines when the voltage starts to burst is identified with the basin boundary between two attractors associated with the active and silent phases. In reality, however, the bursting threshold is a more complicated object. Numerical methods recently developed by the authors approximate the bursting threshold as a locally separating stable manifold of the full slow-fast system. Here, we use these numerical techniques to investigate how a bursting periodic orbit interacts with this stable manifold. We focus on a Morris–Lecar model, which is three dimensional with one slow and two fast variables, as a representative example. We show how the locally separating stable manifold organises the number of spikes in a bursting periodic orbit, and illustrate its role in a spike-adding transition as a parameter is varied.

1 Introduction

Many natural phenomena can be thought of as arising from the coupling of two or more processes that evolve on different time scales. The behaviour of neurons is a particularly good example; in neurons, fluctuations in the membrane potential are fast processes organised by a mixture of slow and fast activation kinetics of the channels that regulate the ionic currents through the cell membrane [11]. Mathematical

[a] e-mail: h.m.osinga@auckland.ac.nz

models of neurons are, therefore, frequently written as systems of ordinary differential equations in which the separation of time scales between the different biological processes is captured by one or more ratios between the time scales of evolution of the variables of the model; such models are called *slow-fast* systems. Nontrivial solutions of such systems consist of segments representing active and silent phases connected via fast transitions.

A common approach for studying slow-fast systems provides insight into the dynamics by investigating the so-called fast and slow subsystems. The fast subsystem is obtained by considering only the fast variables and treating the slow variables as parameters. The bifurcation diagram of the fast subsystem with respect to these slow variables characterises how solutions of the full system may switch between different coexisting attractors of the fast subsystem, which exist as families with respect to the slow variables. The slow subsystem determines the direction in which the full system tracks the families of attractors of the fast subsystem, and in which order the switches between attractors are made. These subsystems represent two different singular limits in which the time-scale ratio between the slow and fast variables is set to zero. In the 1970s, Rinzel [18] utilised this approach to classify neuronal bursting patterns in terms of the bifurcation diagram of the underlying fast subsystem.

In this paper, we consider a three-dimensional slow-fast system with a single slow variable; more precisely, we consider a three-dimensional version of the Morris–Lecar model [16] that was introduced in [19]. The fast subsystem of this model depends on one parameter, and the bifurcations involve only equilibria and periodic orbits. The one-parameter family of equilibria of the fast subsystem is called the critical manifold. This critical manifold is folded and one of its branches of attracting equilibria is associated with the silent phase. The active phase is organised by a one-parameter family of attracting periodic orbits. The families of attracting equilibria and periodic orbits are separated by a branch of saddle equilibria, and the associated family of stable manifolds of these saddle equilibria forms the basin boundary between the two coexisting families of attractors.

Fenichel [8,9] showed that branches of the critical manifold that satisfy certain properties persist as so-called slow manifolds of the full system with time-scale ratio $\varepsilon > 0$, provided ε is small enough. In particular, a branch that consists entirely of saddle-type equilibria of the fast subsystem persists as a saddle slow manifold (SSM). Moreover, the family of stable manifolds of a branch of saddle equilibria also persist as a stable manifold of an SSM. This manifold may act as a local separatrix in phase space, for instance, between the active and silent phases of a bursting orbit [12]. Terman [20] and Lee and Terman [15] show that a bursting periodic orbit keeps bursting as long as it lies (locally) on the "jump-up" side of the separating manifold. In such examples, the number of spikes in a burst is directly related to the interaction between the bursting periodic orbit and the separating stable manifold of an SSM.

Recently, we developed an algorithm for computing the stable manifold of an SSM by continuation of a one-parameter family of orbit segments that are solutions of a two-point boundary value problem [7]. In this paper, we utilise this new computational tool and investigate the geometry of the separating stable manifold in the presence of a bursting periodic orbit for the three-dimensional Morris–Lecar model. As expected from the examples in [7], we find that the separating manifold divides the phase space into different regions connected via a spiral. We also note that the nature of the separating manifold must be such that the periodic orbit can switch between active and silent phases. By varying the time-scale ratio ε, one can control the number of spikes in a burst. We find that the onset of a new spike occurs when the bursting periodic orbit tracks the SSM, that is, when it lies on the stable manifold of the SSM [7,15,17,20].

This paper is organised as follows. In Section 2, we introduce the three-dimensional Morris–Lecar model and review the presence of multi-spike periodic bursting. In

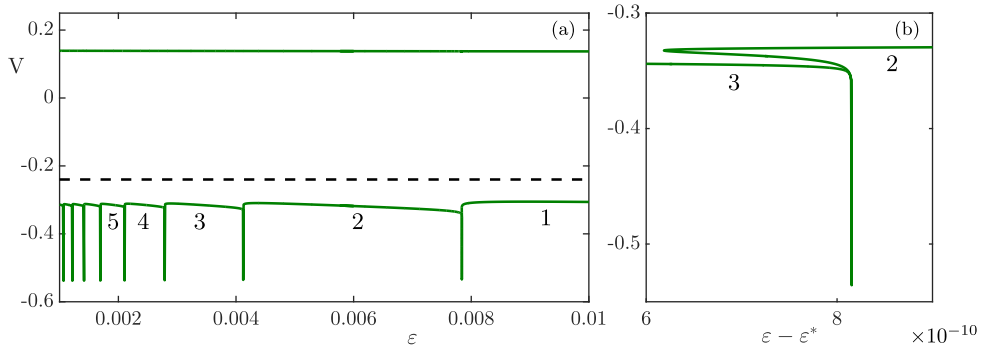

Fig. 1. Bifurcation diagram of system (1) with respect to the time-scale ratio ε; the vertical axis represents the maximum and minimum values of V. Panel (a) shows the range $0.001 < \varepsilon < 0.01$ and panel (b) is an enlargement of the transition for the bursting periodic orbit from two to three spikes; here, the horizontal axis is $\varepsilon - \varepsilon^*$, with $\varepsilon^* = 4.122355 \times 10^{-3}$. The dashed curve corresponds to the saddle equilibrium and the solid curves to the bursting periodic orbit Γ; the numbers along the branch segments indicate how many spikes there are in the burst.

Section 3, we briefly describe the algorithm from [7] that we use to compute the stable manifold of an SSM in the Morris–Lecar model. Section 4 presents the results, which are consistent with the theory, and explain how the structure and geometry of the separating manifold is key to determining the number of spikes in a bursting periodic orbit. Finally, we draw conclusions in Section 5.

2 The three-dimensional Morris–Lecar model

As a representative example of a model of neuronal behaviour, we consider a three-dimensional version of the Morris–Lecar model [16] that was introduced by Rinzel and Ermentrout [19]:

$$\begin{cases} \dot{V} = I - 0.5(V + 0.5) - 2w\,(V + 0.7) - 0.5\left[1 + \tanh\left(\dfrac{V + 0.01}{0.15}\right)(V - 1)\right], \\ \dot{w} = 1.15\left(0.5\left[1 + \tanh\left(\dfrac{V + 0.01}{0.15}\right)\right] - w\right)\cosh\left(\dfrac{V - 0.1}{0.29}\right), \\ \dot{I} = \varepsilon\,(-0.24 - V). \end{cases} \tag{1}$$

The parameter ε represents the time-scale ratio between the slow and fast variables; we assume $0 < \varepsilon \ll 1$, in which case the variables V and w evolve much faster than I. Figure 1 shows a bifurcation diagram of system (1), in which the V-coordinate for the equilibria and the maximum and minimum V-coordinates for the periodic orbits are plotted versus ε. System (1) has a unique equilibrium, denoted E_1, that does not depend on ε and is always a saddle. Co-existing with this equilibrium is a periodic orbit; the orbit has just one spike if ε is large enough, but as ε decreases, additional spikes are added to create a well-defined active burst followed by a silent phase. These spikes are added one at a time via pairs of saddle-node bifurcations of periodic orbits. That is, there exists an exponentially small ε-interval during which an attracting periodic orbit with n spikes co-exists with an attracting periodic orbit with $n + 1$ spikes, together with a saddle-type periodic orbit. Figure 1b shows an enlargement of this transition for the case $n = 2$. The width of the ε-interval is of

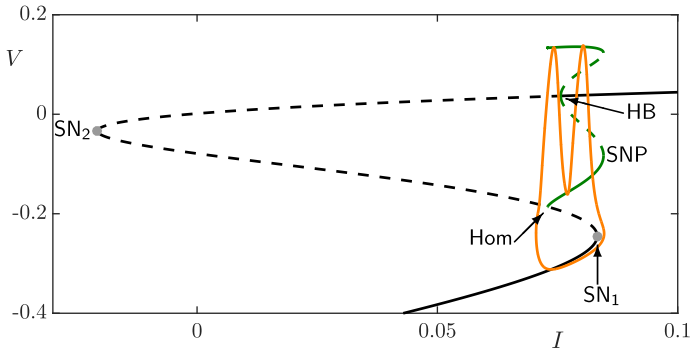

Fig. 2. A bursting periodic orbit (orange) of system (1) with $\varepsilon = 0.005$, superimposed on the bifurcation diagram of the fast subsystem in the (I, V)-plane.

order 10^{-10}, and the spike-adding transition occurs approximately for $4.122355619 \times 10^{-3} \leq \varepsilon \leq 4.122355815 \times 10^{-3}$; hence, if we define $\varepsilon^* = 4.122355 \times 10^{-3}$, then we have $6.19 \times 10^{-10} \leq \varepsilon - \varepsilon^* \leq 8.15 \times 10^{-10}$, approximately, during this transition.

We obtain the two-dimensional fast subsystem by taking the singular limit $\varepsilon \to 0$ in system (1). In this limit, the slow variable I can be viewed as a parameter. Figure 2 shows the two-spike bursting periodic orbit (orange) Γ that exists for system (1) when $\varepsilon = 0.005$; the bifurcation diagram of the fast subsystem of (1) is overlayed on Γ. As for Figure 1, solid and dashed curves indicate stable and unstable families of equilibria and/or periodic orbits, respectively; the periodic orbits are again represented by their maximum and minimum V-values. The critical manifold is an S-shaped branch of equilibria; they are stable on the lower branch and change to saddle type at a saddle-node bifurcation, denoted SN_1. Another saddle-node bifurcation, denoted SN_2, separates the saddle branch from the unstable equilibria on the upper branch. These equilibria become stable as they go through a subcritical Hopf bifurcation HB. The family of periodic orbits (green) emanating from the Hopf bifurcation are unstable. After a saddle-node bifurcation of periodic orbits (SNP), the periodic orbits become stable and terminate at a homoclinic bifurcation, denoted Hom, as they collide with the saddle branch.

Note that I is increasing if $V < -0.24$, which means that Γ tracks the lower attracting branch up to SN_1, jumps up to the family of attracting periodic orbits, after which $\dot{I} < 0$ and Γ tracks this family in the direction of decreasing I until it reaches Hom; then Γ drops back down to the lower attracting branch and the trajectory repeats. The bursting periodic orbit for $\varepsilon = 0.005$ exhibits two spikes during the burst. Figure 2 suggests that the number of spikes increases as ε decreases, because a slower drift to the left for I will result in a larger number of oscillations around the branch of attracting periodic orbits of the fast subsystem. However, the precise geometric mechanism that causes Γ to exhibit two spikes for this value of ε cannot be inferred from this figure.

Just as for the systems in [15,20], the stable manifold of an SSM locally divides the phase space; a bursting orbit bursts when it (locally) lies on one side of the stable manifold of the SSM and becomes quiescent when it moves to the other side. Our main goal is to compute this separatrix for system (1) with $\varepsilon = 0.005$, and investigate its geometric nature. We first give a brief description of the algorithm used.

3 The stable manifold of a saddle slow manifold

Fenichel theory guarantees that branches of the critical manifold of system (1) consisting of equilibria with the same stability type persist as slow manifolds for $\varepsilon > 0$,

provided ε is small enough [8,9]; in particular, the branch of saddle-type equilibria persists as an SSM. We note that SSMs are not unique. Instead, there exists a family of one-dimensional SSMs that all lie exponentially close to one another [9]. Each such SSM has corresponding (non-unique) two-dimensional stable and unstable manifolds, which consist of trajectories that converge to the SSM in backward and forward time, respectively.

Guaranteed existence of an invariant slow manifold does not mean that it is straightforward to compute such a manifold. The numerical approximation of an SSM is a particular challenge, because such a manifold has both repelling and attracting fast directions, which results in an exponentially fast accumulating numerical error; classical initial value problem solvers tend not to work in this setting, even when extremely small step sizes are used. There are well-established numerical methods for computing attracting and repelling slow manifolds [1,2], but methods for the approximation of SSMs are scarce and we know of only two other methods for approximating the stable manifold of an SSM. Guckenheimer and Kuehn [10] approximate the SSM as an orbit segment that starts or ends on the saddle branch of the critical manifold. Its stable manifold is then computed by backward-time integration, starting a small distance away from the computed SSM in the direction of the stable eigenvectors of the corresponding branch of saddle equilibria of the fast subsystem. This method induces a numerical error that depends explicitly on how far the system is perturbed from the singular limit $\varepsilon = 0$; see also [3] for a similar approach. Kristiansen [14] approximates the SSM with an iterative method applied to an algebraic invariance equation. Its stable manifold is then computed by a different iterative method based on projection onto the SSM and another projection normal to it. The convergence of the iterative schemes is guaranteed if ε is small enough.

In this section, we present a brief review of the two-point boundary value problem (2PBVP) set-up introduced in [7] that we use for the computation of the two-dimensional stable manifold of an SSM. Our approach is different from the 2PBVP approaches described in [3,10] and does not use elements defined with respect to the fast subsystem; it can be applied for any value of ε, though the accuracy of the computation will decrease as ε increases into a regime where the system ceases to exhibit a separation of time scales.

We consider a particular SSM, denoted $S^{\mathrm{x}}_{\varepsilon}$, and a particular associated stable manifold, denoted $W^s(S^{\mathrm{x}}_{\varepsilon})$, as the object that we wish to approximate numerically. Loosely speaking, $S^{\mathrm{x}}_{\varepsilon}$ is the orbit segment that remains close to (the saddle branch of) the critical manifold for the longest possible time; its associated stable manifold consists of all orbit segments that, upon entering a small neighbourhood of $S^{\mathrm{x}}_{\varepsilon}$, converge very quickly towards $S^{\mathrm{x}}_{\varepsilon}$, follow it for a time interval of $O(1)$ on the slow time scale, and then diverge from $S^{\mathrm{x}}_{\varepsilon}$ along an unstable direction, again very quickly [13]. We approximate $W^s(S^{\mathrm{x}}_{\varepsilon})$ in a given region of interest as a one-parameter family of orbit segments that have the following special property: when the orbit segment comes close to the corresponding saddle branch S^{x}_0 of the critical manifold, it remains close for the longest possible time compared with other orbit segments that come equally close to S^{x}_0. By formulating appropriate boundary conditions, we set up a 2PBVP that has a one-parameter solution family, which is solved for by continuation with the software package AUTO [4,5].

The computation of orbit segments of system (1) is done in the time-rescaled system

$$\dot{\mathbf{u}} = T\,F(\mathbf{u}), \tag{2}$$

where $\mathbf{u} = (V, w, I) \in \mathbb{R}^3$ and $F : \mathbb{R}^3 \to \mathbb{R}^3$ is the right-hand side of system (1). Then, each orbit segment of the rescaled system (2) is defined on the time interval $[0, 1]$, and corresponds to an orbit segment of the original system (1) defined on $[0, T]$. The

advantage of this rescaling is that one can now impose boundary conditions at $t = 0$ and $t = 1$, and the total integration time T is solved for as part of the 2PBVP. An orbit segment of system (2) for a given integration time T is (locally) uniquely defined if we impose k boundary conditions at $t = 0$ and $3 - k$ boundary conditions at $t = 1$, where $0 \leq k \leq 3$. Note that the cases $k = 0$ and $k = 3$ are initial value problems in backward and forward time, respectively.

The family of orbit segments that defines $W^s(S^{\mathrm{x}}_\varepsilon)$ is obtained via continuation from a first solution that satisfies the 2PBVP. This first orbit segment is computed with a homotopy step that consists of two parts; we have $k = 1$ in part one and $k = 2$ in part two. Note that the saddle branch S^{x}_0 of the critical manifold of system (1) is one dimensional and we can associate a direction to it that agrees with the nearby direction of the flow. We initialise system (2) at a point as close as possible to the end of S^{x}_0. We set $k = 1$ and extract an orbit segment from this point such that the end point stays very close to S^{x}_0 and the initial point is constrained to a plane while T is increasing from 0. The problem is well posed if we allow the end point to move only along a line. In part two, we set $k = 2$ and allow the initial condition to move along a line only. The boundary condition at $t = 1$ restricts the end point to a plane, and we vary T until AUTO detects a maximum with respect to the total integration time; the result is that the end point has moved away from S^{x}_0 in the direction of the unstable manifold of $S^{\mathrm{x}}_\varepsilon$, but the orbit segment has a sub-segment that remains close to S^{x}_0 for the longest time. This orbit segment is part of the family that defines $W^s(S^{\mathrm{x}}_\varepsilon)$.

We obtain the entire family as follows. We switch back to $k = 1$, but also keep a single boundary condition at $t = 1$. The additional constraint at $t = 1$ is that T remains maximal, which is detected as a fold bifurcation in two parameters; these two parameters are the two coordinates that identify the initial point in the plane defined by the boundary condition at $t = 0$. The union of all the orbit segments with maximal integration time computed this way form the two-dimensional stable manifold of $S^{\mathrm{x}}_\varepsilon$. We refer to [7] for more specific details on the 2PBVP set-up.

4 Interactions between $W^s(S^{\mathrm{x}}_\varepsilon)$ and the bursting periodic orbit Γ

We now compute $W^s(S^{\mathrm{x}}_\varepsilon)$ for the Morris–Lecar model (1) with $\varepsilon = 0.005$. The bursting periodic orbit Γ for this value of ε has two spikes in the active phase and $W^s(S^{\mathrm{x}}_\varepsilon)$ is, locally, the separatrix between the active and silent phases. Figure 3 shows the stable manifold $W^s(S^{\mathrm{x}}_\varepsilon)$ (blue surface) of $S^{\mathrm{x}}_\varepsilon$ together with Γ (orange curve); the black curve is the critical manifold and the saddle equilibrium E_1 (green $\times$) is located on the middle branch. We also plot the one-dimensional stable manifold $W^s(\mathsf{E}_1)$ (cyan curve) of E_1, one branch of which extends directly to ∞, while the other exhibits a large loop around the upper branch of the critical manifold before extending to ∞ as well. The SSM $S^{\mathrm{x}}_\varepsilon$ is contained in $W^s(S^{\mathrm{x}}_\varepsilon)$, so that $W^s(S^{\mathrm{x}}_\varepsilon)$ has two sheets, one on either side of $S^{\mathrm{x}}_\varepsilon$. Like $W^s(\mathsf{E}_1)$, one sheet of $W^s(S^{\mathrm{x}}_\varepsilon)$ goes directly to ∞, but the other sheet wraps around the upper branch of the critical manifold. Hence, this sheet consists of layers that divide the phase space into different regions connected through spirals. When followed backward in time, the orbit segments of $W^s(S^{\mathrm{x}}_\varepsilon)$ spiral out and away from the upper branch of the critical manifold.

Note from Figure 3 that a few of the outer layers of $W^s(S^{\mathrm{x}}_\varepsilon)$ accumulate onto $W^s(\mathsf{E}_1)$, rather than extending to ∞. Indeed, it is to be expected that $W^s(S^{\mathrm{x}}_\varepsilon)$ intersects the two-dimensional unstable manifold $W^u(\mathsf{E}_1)$ of the saddle E_1, which means that there exist orbit segments on $W^s(S^{\mathrm{x}}_\varepsilon)$ that come from E_1. Consequently, there must exist nearby orbit segments on $W^s(S^{\mathrm{x}}_\varepsilon)$ that pass arbitrarily close by E_1, which implies that they lie arbitrarily close to $W^s(\mathsf{E}_1)$ when followed backward in time.

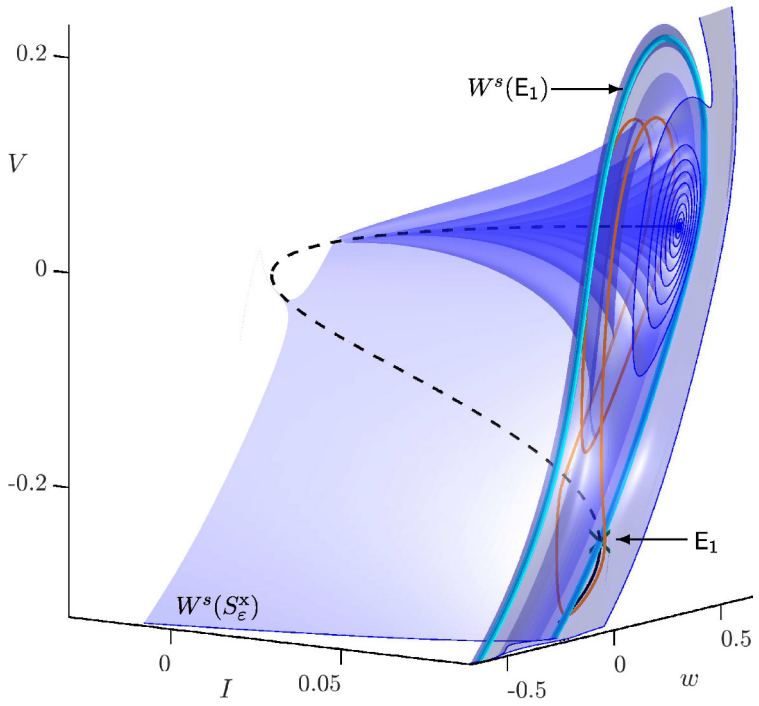

Fig. 3. The stable manifold $W^s(S^{\mathrm{x}}_\varepsilon)$ (blue) of $S^{\mathrm{x}}_\varepsilon$ together with the bursting periodic orbit Γ (orange) of system (1) for $\varepsilon = 0.005$. The saddle equilibrium E_1 (green $\times$) with one-dimensional stable manifold $W^s(\mathsf{E}_1)$ (cyan) lies on the middle branch of the critical manifold (black).

Figure 3 illustrates that the accumulation onto $W^s(\mathsf{E}_1)$ in backward time affects only a finite number of layers of $W^s(S^{\mathrm{x}}_\varepsilon)$, such that when Γ comes close to E_1 in the silent phase, it can go around $W^s(\mathsf{E}_1)$ to the other side of $W^s(S^{\mathrm{x}}_\varepsilon)$ and enter the active phase.

Figure 4 illustrates the separating nature of $W^s(S^{\mathrm{x}}_\varepsilon)$ in more detail. To obtain this figure, we used the plane $V = 0.1$ to define a slice through the phase space. The upper panel of the figure shows the intersections of $W^s(S^{\mathrm{x}}_\varepsilon)$ with this plane as thick (black) curves, and those of $W^s(\mathsf{E}_1)$ as cyan dots; the intersections of Γ with the plane are denoted by the (orange) symbols $\odot$ or $\otimes$, respectively, depending on whether the flow at these points is increasing or decreasing with respect to V. The lower panel shows the portions of $W^s(S^{\mathrm{x}}_\varepsilon)$ and $W^s(\mathsf{E}_1)$ with $V \leq 0.1$ in the full phase space, along with Γ (orange); the intersections of $W^s(S^{\mathrm{x}}_\varepsilon)$ with the plane are highlighted with thick curves for ease of visualisation. Note how precisely two layers of $W^s(S^{\mathrm{x}}_\varepsilon)$ (blue) spiral around and accumulate on $W^s(\mathsf{E}_1)$ (cyan). A point starting on Γ in the silent phase lies behind $W^s(S^{\mathrm{x}}_\varepsilon)$ with respect to the view point shown in Figure 4. It can move past the top two layers of $W^s(S^{\mathrm{x}}_\varepsilon)$ by going around the back branch of $W^s(\mathsf{E}_1)$ near E_1, thereafter entering the active phase. In the active phase, Γ makes one oscillation following the spiralling orbit segments of $W^s(S^{\mathrm{x}}_\varepsilon)$, and a second oscillation to reach the back side of $W^s(S^{\mathrm{x}}_\varepsilon)$ so that it can close up again.

Decreasing ε increases the number of spikes in the active phase of Γ. Intuitively, this is because the drift in I is slower and there is more time to oscillate around the family of attracting periodic orbits of the fast subsystem. Recall from Figure 1 that the generation of a new spike involves a pair of saddle-node bifurcations of periodic

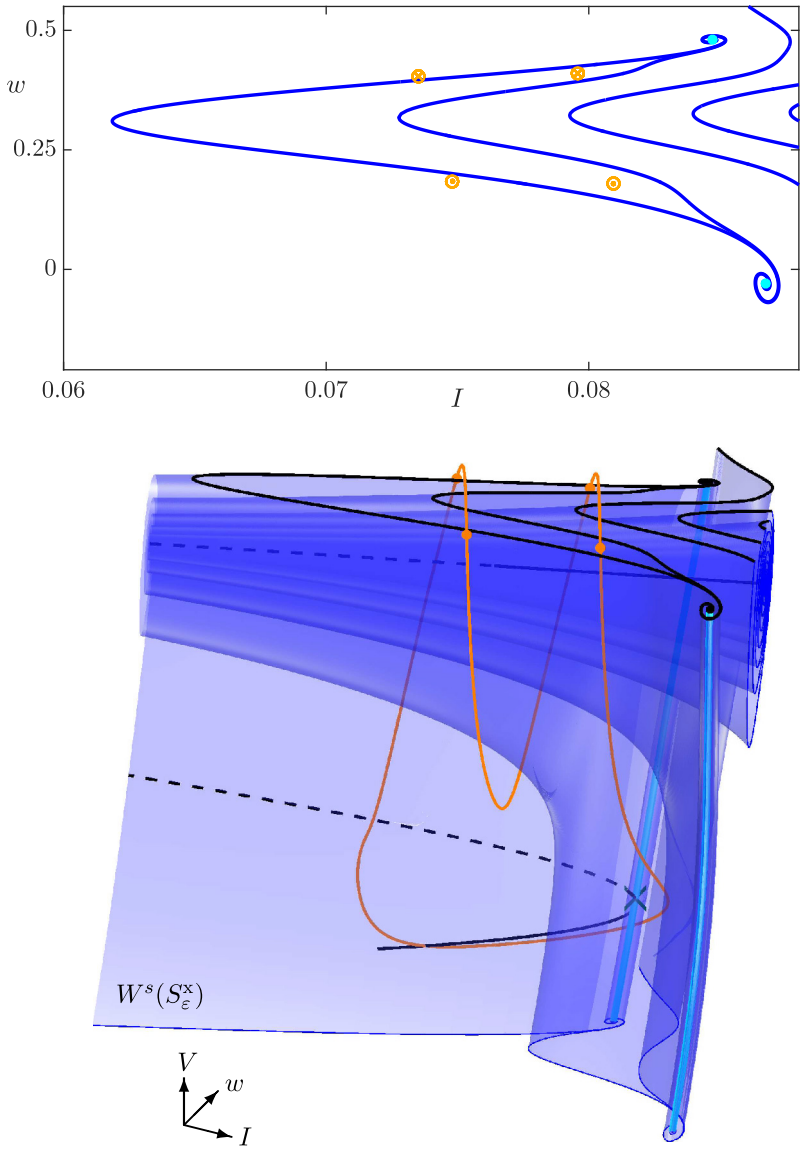

Fig. 4. Intersections of $W^s(S^x_\varepsilon)$ (blue) and $W^s(\mathsf{E}_1)$ (cyan) with the section $V = 0.1$, shown in projection onto the (I, w)-plane (top) and in the full phase space for the part of $W^s(S^x_\varepsilon)$ and the segments of $W^s(\mathsf{E}_1)$ with $V \leq 0.1$ (bottom); also shown are Γ (orange) and its intersections with $V = 0.1$, where $\odot$ and $\otimes$ indicate whether the flow at the intersection point is increasing or decreasing with respect to V, respectively.

orbits such that three periodic orbits (two stable and one unstable) coexist in an exponentially small parameter interval. In this spike-adding interval, $W^s(S^x_\varepsilon)$ exhibits a dramatic geometric change that is extremely difficult to capture numerically, because the parameter variation is smaller than the computational precision of the manifold. We computed $W^s(S^x_\varepsilon)$ for $\varepsilon = \varepsilon^* + 8.15 \times 10^{-10} = 4.122355815$, as shown in Figure 5; here, we show only the two-spike periodic orbit using the same slices as in Figure 4. Observe that Γ traces S^x_0 (dashed black curve) in the bottom panel. The value of ε is

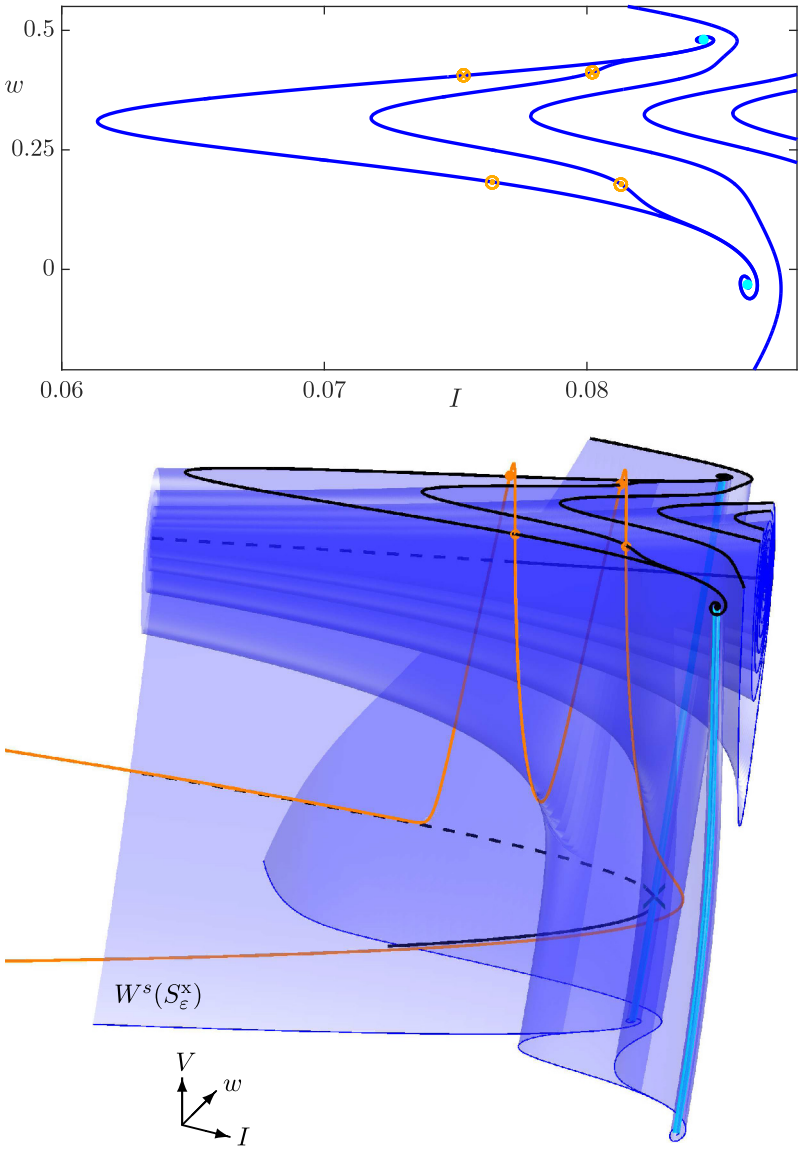

Fig. 5. The stable manifold $W^s(S^x_\varepsilon)$ (blue) together with the bursting periodic orbit Γ (orange) of system (1) for $\varepsilon = \varepsilon^* + 8.15 \times 10^{-10}$, approximately at the second saddle-node bifurcation of periodic orbits where the two-spike bursting periodic orbit disappears; see Figure 1. Shown are the intersections of $W^s(S^x_\varepsilon)$ (blue) and $W^s(\mathsf{E}_1)$ (cyan) with the section $V = 0.1$ in projection onto the (I, w)-plane (top) and in the full phase space for the part of $W^s(S^x_\varepsilon)$ and the segments of $W^s(\mathsf{E}_1)$ with $V \leq 0.1$ (bottom); see also Figure 4.

such that Γ follows S^x_0 for the longest possible time, which means that $\Gamma \subset W^s(S^x_\varepsilon)$ by definition of $W^s(S^x_\varepsilon)$; this value of ε is almost the same as the value for the second saddle-node bifurcation of periodic orbits that destroys the two-spike periodic orbit Γ. Unfortunately, the other two coexisting periodic orbits are indistinguishable on the scale of the enlargement shown in Figure 5. Their significant difference is in the way they first move up and only then drop down to the lower branch, far to the left of the regime shown in Figure 5.

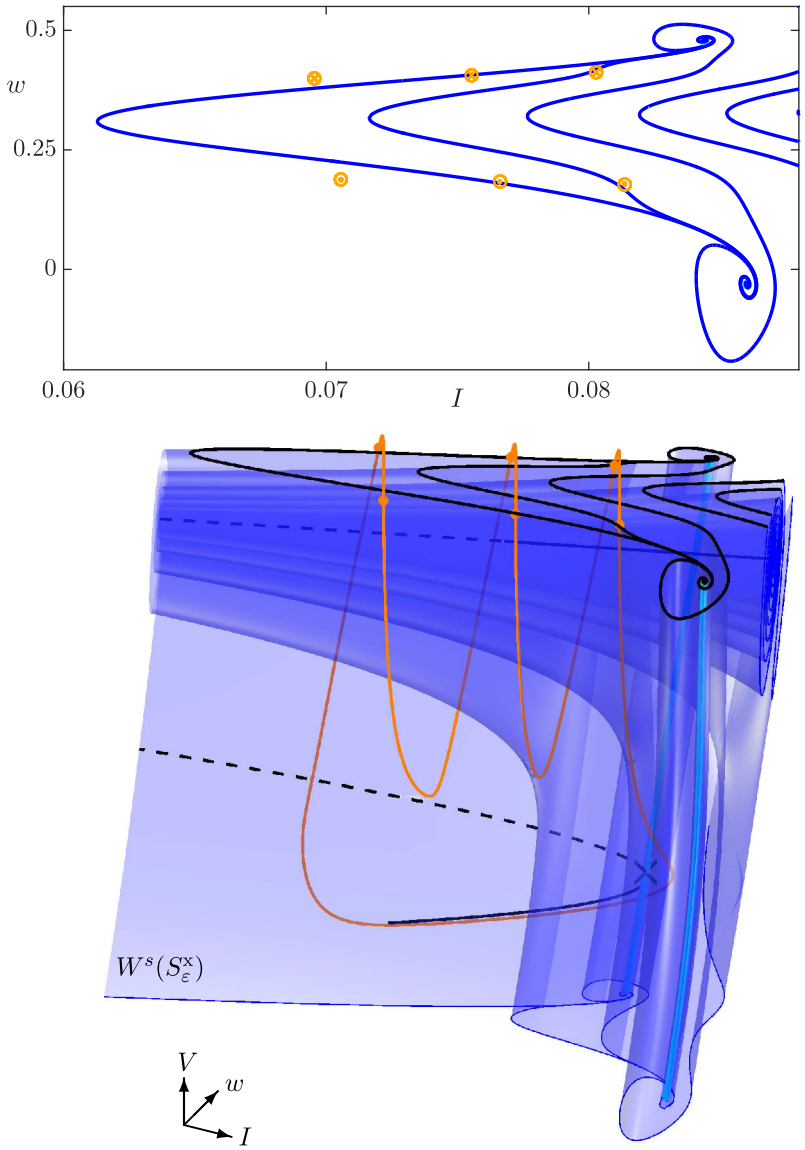

Fig. 6. The stable manifold $W^s(S^{\mathrm{x}}_\varepsilon)$ (blue) together with the bursting periodic orbit Γ (orange) of system (1) for $\varepsilon = 0.004$, when a three-spike bursting periodic orbit exists. Shown are the intersections of $W^s(S^{\mathrm{x}}_\varepsilon)$ (blue) and $W^s(\mathsf{E}_1)$ (cyan) with the section $V = 0.1$ in the projection onto the (I, w)-plane (top) and in the full phase space for the part of $W^s(S^{\mathrm{x}}_\varepsilon)$ and the segments of $W^s(\mathsf{E}_1)$ with $V \leq 0.1$ (bottom); see also Figures 4 and 5.

Geometrically, the layers of $W^s(S^{\mathrm{x}}_\varepsilon)$ compress towards smaller values of I. Hence, Γ crosses $W^s(S^{\mathrm{x}}_\varepsilon)$ as we follow Γ along the S-shaped branch. As soon as Γ crosses $W^s(S^{\mathrm{x}}_\varepsilon)$, a new spike is generated. Figure 6 shows $W^s(S^{\mathrm{x}}_\varepsilon)$ and Γ for $\varepsilon = 0.004$, when Γ is a three-spike periodic orbit; here, we show the same slices as in Figures 4 and 5. Observe that now the first three outer layers of $W^s(S^{\mathrm{x}}_\varepsilon)$ accumulate onto $W^s(\mathsf{E}_1)$; as before, Γ moves past these layers of $W^s(S^{\mathrm{x}}_\varepsilon)$ by going around the back branch of $W^s(\mathsf{E}_1)$ near E_1, resulting in three oscillations during the active phase before the orbit reaches the back side of $W^s(S^{\mathrm{x}}_\varepsilon)$ again.

5 Conclusions

We computed the stable manifold $W^s(S^{\mathrm{x}}_\varepsilon)$ of a saddle slow manifold for the three-dimensional Morris–Lecar system (1), given in [19], to investigate its role in organising the number of spikes in the active phase of a bursting periodic orbit Γ. The computations were done with the algorithm presented in [7]. Our computations showed the significant difference in the structure of the top two layers of $W^s(S^{\mathrm{x}}_\varepsilon)$ when compared with the other layers, if $\varepsilon = 0.005$ and Γ exhibits two spikes in the active phase. The first two layers accumulate onto the one-dimensional stable manifold of the saddle equilibrium, while the other layers spread out to ∞ in backward time. The location of Γ when it enters the active phase, relative to these layers of $W^s(S^{\mathrm{x}}_\varepsilon)$, dictates the number of spikes in the burst.

We varied ε to illustrate how $W^s(S^{\mathrm{x}}_\varepsilon)$ interacts with Γ during a spike-adding transition. We showed numerical results specifically for the case of the transition from two to three spikes, but our computations suggest that the results are qualitatively the same for other spike-adding transitions as well. Our results not only explain the role of $W^s(S^{\mathrm{x}}_\varepsilon)$ in a spike-adding transition, but also provide evidence for the accuracy of the computations. Indeed, for the case of the transition from two to three spikes, $\Gamma \subset W^s(S^{\mathrm{x}}_\varepsilon)$ precisely for the value of ε that we expected.

This work complements the results presented in [6,7], where we considered slow-fast systems that exhibit bursting in the transient behaviour observed after a large perturbation. The global attractor for the system studied in [6,7] is an equilibrium state rather than a periodic orbit as for the example in this paper. However, as defined in [12], the stable manifold of an SSM plays a similar role; specifically, it acts as the excitability threshold of the system that controls the occurrence of transient bursts as well as the number of spikes exhibited during a burst. We note that bursting is not always a periodic phenomenon; for instance, the number of spikes in a bursting orbit may change in a non-periodic manner from burst to burst. We conjecture that similar considerations about the role of SSMs would be relevant in explaining the occurrence of non-periodic bursting, but leave this exploration for future work.

References

1. M. Desroches, J. Guckenheimer, B. Krauskopf, C. Kuehn, H.M. Osinga, M. Wechselberger, SIAM Rev. **54**, 211 (2012)
2. M. Desroches, B. Krauskopf, H.M. Osinga, SIAM J. Appl. Dyn. Syst. **7**, 1131 (2008)
3. M. Desroches, B. Krauskopf, H.M. Osinga, Discr. Contin. Dyn. Syst. S **2**, 807 (2009)
4. E.J. Doedel, Congr. Numer. **30**, 265 (1981)
5. E.J. Doedel, B.E. Oldeman, AUTO-07p: Continuation and bifurcation software for ordinary differential equations (Concordia University, Montreal, Canada), with major contributions from A.C. Champneys, T.F. Fairgrieve, Yu.A. Kuznetsov, R.C. Paffenroth, B. Sandstede, X.J. Wang, and C. Zhang. Available at http://cmvl.cs.concordia.ca/auto/
6. S. Farjami, V. Kirk, H.M. Osinga, Eur. Phys. J. Special Topics **225**, 2601 (2016)
7. S. Farjami, V. Kirk, H.M. Osinga, SIAM J. Appl. Dyn. Syst. **17**, 350 (2018)
8. N. Fenichel, Indiana Univ. Math. J. **21**, 193 (1972)
9. N. Fenichel, J. Differ. Equ. **31**, 53 (1979)
10. J. Guckenheimer, C. Kuehn, SIAM J. Appl. Dyn. Syst. **8**, 854 (2009)
11. A.L. Hodgkin, A.F. Huxley, J. Physiol. **117**, 500 (1952)
12. E.M. Izhikevich, *Dynamical Systems in Neuroscience: The Geometry of Excitability and Bursting* (The MIT Press, 2007)
13. C.K.R.T. Jones, N. Kopell, J. Differ. Equ. **108**, 64 (1994)
14. K.U. Kristiansen, SIAM J. Appl. Dyn. Syst. **14**, 1189 (2015)
15. E. Lee, D. Terman, J. Differ. Equ. **158**, 48 (1999)

16. C. Morris, H. Lecar, Biophys. J. **35**, 193 (1981)
17. H.M. Osinga, K.T. Tsaneva-Atanasova, Chaos **23**, 046107 (2013)
18. J. Rinzel, A formal classification of bursting mechanisms in excitable systems, in *Proc. Int. Congress Math.*, edited by A.M. Gleason (1986), Vol. 2, pp. 1578–1593
19. J. Rinzel, B. Ermentrout, Analysis of neural excitability and oscillations, in *Methods of Neural Modeling: From Synapses to Networks*, edited by C. Koch, I. Segev (1989), pp. 135–169
20. D. Terman, SIAM J. Appl. Math. **51**, 1418 (1991)